Lefkimmiatis et al., http://www.jcb.org/cgi/content/full/jcb.201303159/DC1

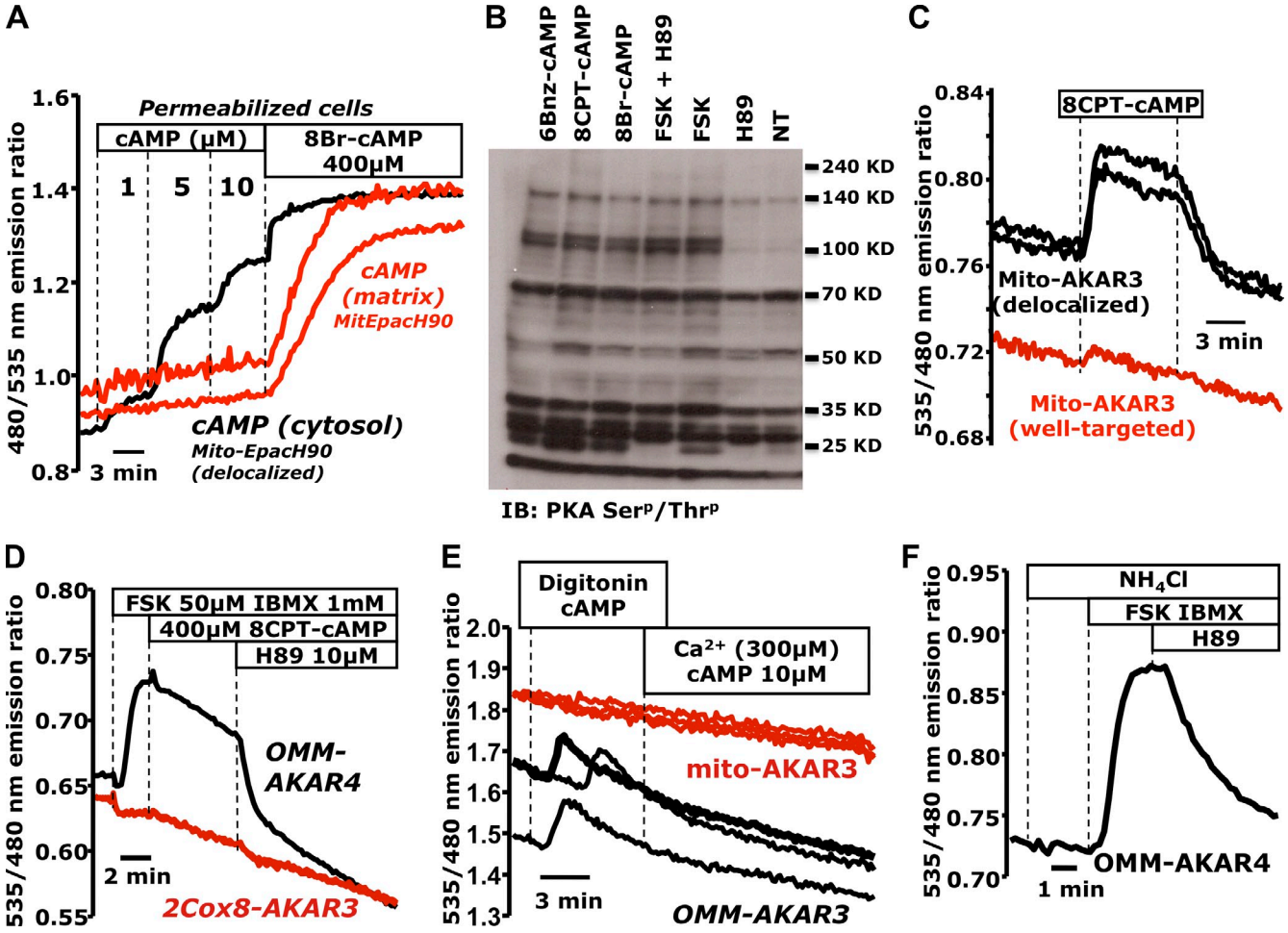

Figure S1. **Validation of mito-EpacH90 and AKAR-based sensors targeted to mitochondria.** (A) To assess the cAMP sensitivity of mito-EpacH90, we took advantage of the small number of cells (~5%) in which the overexpressed sensor was poorly localized, resulting in probe within both mitochondria and cytosol. Permeabilized cells expressing well-targeted mito-EpacH90 (two representative cells; red traces) responded only to 8Br-cAMP, and not to exogenous cAMP. However, permeabilized cells in the same microscope field with delocalized sensor reported cAMP concentrations from 1 µM to 10 µM, well within the range of the parent probe EpacH90 (one representative cell; black trace). Data presented are from a single representative experiment out of four repeats (20 mito-EpacH90 cells, 4 nontargeted cells). (B) HEK cells were treated with cell-permeant cAMP analogues (10 nM 6Bnz-cAMP-AM, 1 mM 8CPT-cAMP, or 1 mM 8Br-cAMP), or with saturating concentrations of FSK (50 µM), the latter either alone or in the presence of the PKA inhibitor H89 (10 µM). PKA-dependent phosphorylation patterns were detected in total cell lysates (10–20 µg) by Western blotting using the Phospho-(Ser/Thr) PKA substrate antibody. The cAMP analogues generated phosphorylation patterns very similar to those of FSK, with 8CPT-cAMP being nominally the most potent; presented here is a single experiment typical of three repeats. (C) In cells in which mito-AKAR3 (two representative cells; black traces) was delocalized (<2% of total cells), the probe responded reversibly to 8CPT-cAMP, which suggests that mito-AKAR3 is functional. Meanwhile, neighboring cells in which mito-AKAR3 was contained within mitochondria (two representative cells; red trace) did not respond. Data shown are from one representative experiment out of four repeats (5 OMM-AKAR3 cells, 10 mito-AKAR3 cells). (D) PKA activity was monitored in mixed populations of HeLa cells expressing AKAR3 targeted to the matrix using a less bulky targeting sequence (2Cox8-AKAR3; two representative cells; red trace) or OMM-AKAR4 (single representative cell; black trace) together with mCherry. It is important to note that the Cox8 targeting motif is cleaved once the sensor reaches the matrix; the data shown are from one representative experiment out of eight repeats (20 2Cox8-AKAR3 cells, 19 OMM-AKAR4 cells). (E) Native cAMP does not induce PKA activity in the mitochondrial matrix. Mixed populations of HeLa cells expressing either mito-AKAR3 (three representative cells; red traces) or OMM-AKAR3 (plus mCherry; three representative cells; black traces) were permeabilized on the microscope stage using digitonin in the presence of 10 µM cAMP. Thanks to the presence of cAMP in the media, we were able to precisely time the moment in which the plasma membrane became permeabilized in individual cells as measured by the activation of OMM-AKAR3 (~3 min). Upon permeabilization, we challenged the cells using 300 µM Ca^{2+} to induce MPT in the continued presence of 10 µM cAMP. We expected mitochondria to undergo permeability transition 1 min into the Ca^{2+} treatment (see Fig. 1 E), an event that would allow cAMP to reach the matrix and activate PKA. However, 5 min of this treatment failed to induce any PKA activity, as measured by mito-AKAR3. Data shown are from one representative experiment out of five repeats (17 mito-AKAR3 cells, 13 OMM-AKAR3 cells). (F) To mimic the alkaline environment of the mitochondrial matrix in HeLa cells expressing OMM-AKAR4, we used 20 mM NH_4Cl to elicit cellular alkalinization (intracellular pH of ~7.8). During this treatment, OMM-AKAR4 responded to FSK and IBMX treatment in an H89-sensitive manner. Data shown are from a single representative experiment out of three repeats (11 cells).

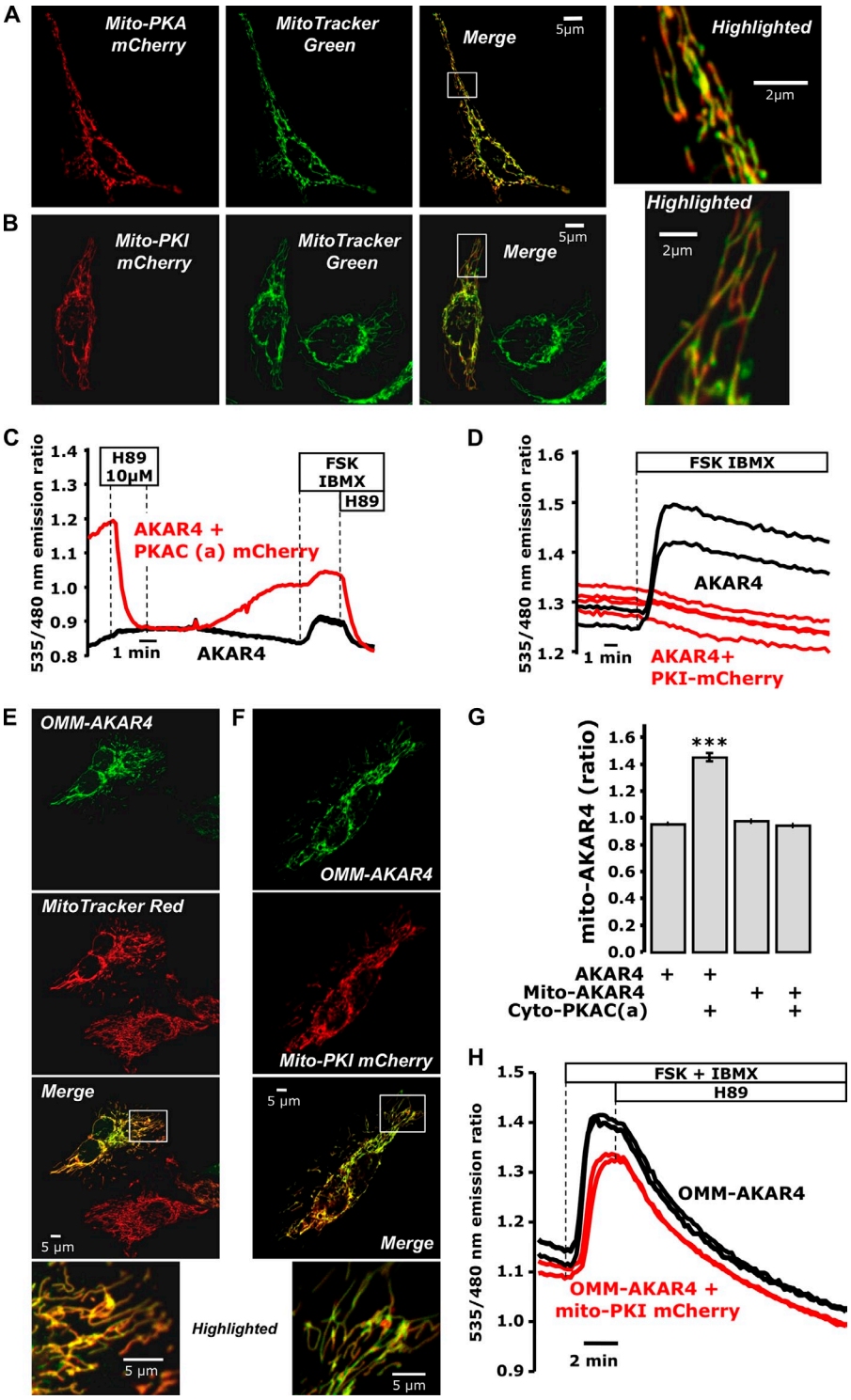

Figure S2. **Mitochondrial targeting and validation of the genetically encoded matrix-targeted PKA inhibitor and catalytic subunit.** (A and B) Live-cell confocal images of HeLa cells expressing mito-PKACat-mCherry (A) or mito-PKI-mCherry (B). Cells were co-loaded with the mitochondrial marker MitoTracker green. (C) Co-expression of cyto-PKACat-mCherry together with the FRET-based PKA activity reporter AKAR4 (single representative cell; red trace) consistently resulted in higher starting FRET ratios (as compared with neighboring cells expressing AKAR4 alone; two representative cells; black trace) that were reversed by the PKA-inhibitor H89. Data shown are from one representative experiment out of five repeats (6 AKAR4 cells, 11 PKACat-mCherry cells). (D) In contrast, when we coexpressed cyto-PKI-mCherry together with AKAR4 (four representative cells; red traces), this construct completely blocked the AKAR4 response to FSK/IBMX, a treatment that consistently saturated AKAR4 (two representative cells; black traces) in neighboring cells that did not express PKI. Data shown are from one representative experiment out of five repeats (11 AKAR4 cells, 16 PKI-mCherry cells). (E) Live-cell confocal images of HeLa cells expressing OMM-AKAR4 and loaded with the mitochondrial marker MitoTracker red. (F) Confocal images of HeLa cells coexpressing OMM-AKAR4 and mito-PKI-mCherry. (G) Bar graph of the starting ratios in cells expressing AKAR4 (54 cells) or mito-AKAR4 alone (81 cells), or together with cytosolic PKACat-mCherry (20 cells). The AKAR4 starting ratio in the presence of the constitutively active catalytic subunit was very high; however, no difference was detected in the mito-AKAR4 ratio in the presence of PKA-Cat-mCherry. Data reflect the mean of all cells (***, $P < 0.0001$). Error bars indicate mean ± SD. (H) Mixed populations of cells expressing OMM-AKAR4 alone (two representative cells; black traces) or coexpressing OMM-AKAR4 and mito-PKI-mCherry (two representative cells; red traces). In all cells, OMM-AKAR4 responded to FSK/IBMX in an H89-sensitive manner, independent of the presence of mito-PKI-mCherry. These experiments demonstrate that mito-PKI-mCherry and OMM-AKAR4 are physically and functionally segregated in the matrix and OMM, respectively, even when overexpressed in the same cell. Data shown are from one representative experiment out of six repeats. Highlighted panels show enlarged views of the boxed regions.

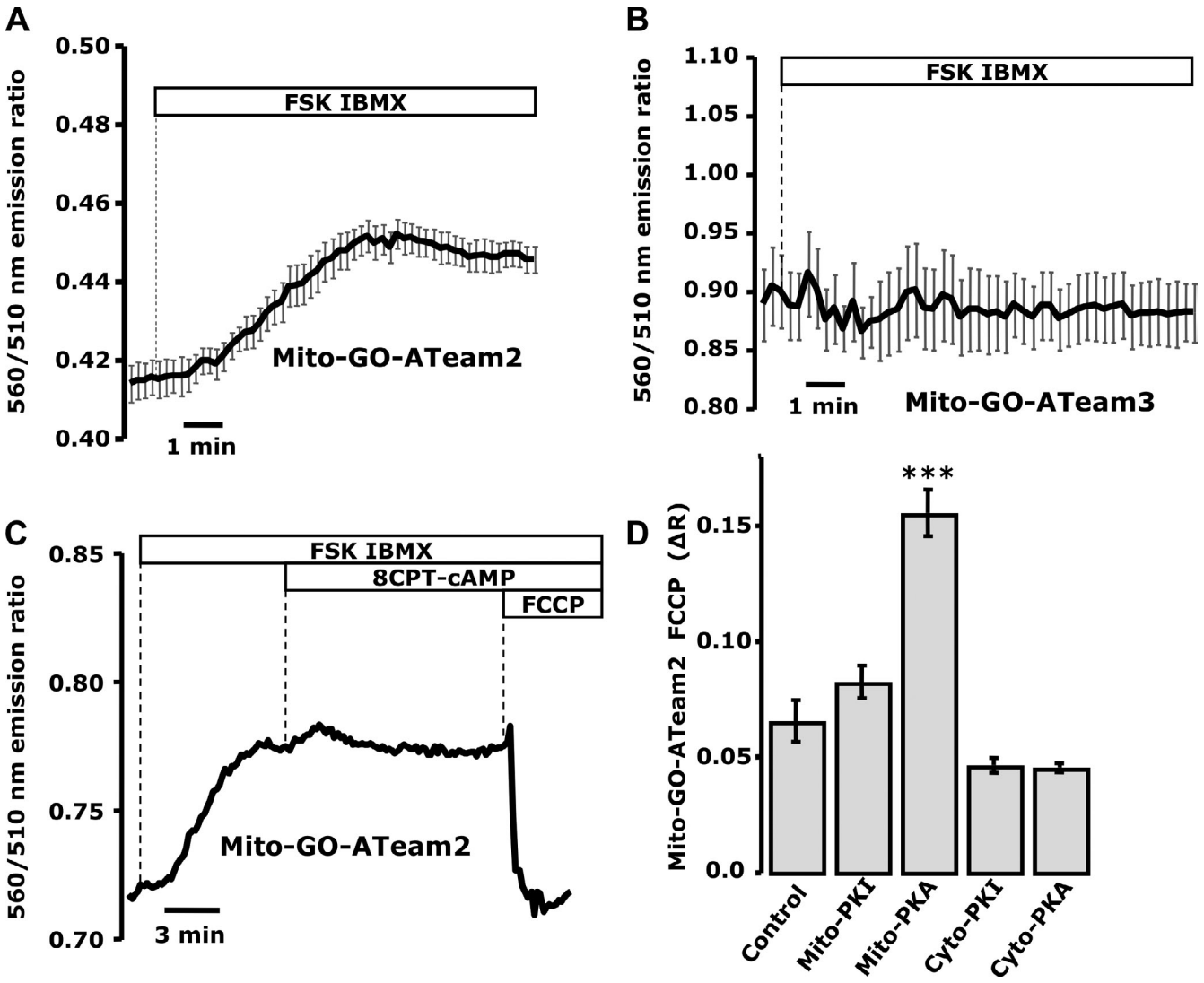

Figure S3. **Mitochondrial ATP measurements in single cells.** HeLa cells expressing mito-GO-ATeam2 or mito-GO-ATeam3 were mounted in a home-built flow-through perfusion chamber, and imaged using 40× or 60× oil immersion objective lenses. 560 nm/510 nm FRET emission ratios were acquired every 5–10 s. (A) Cells expressing the FRET-based ATP sensor GO-ATeam2 targeted to the mitochondrial matrix (mito-GO-ATeam2) consistently responded to treatment with FSK/IBMX, which induced cAMP elevation in the cytosol but not the mitochondrial matrix (n = 12 experiments; 68 mito-GO-ATeam2 cells). (B) Cells expressing the mutant ATP-blind sensor mito-GO-ATeam3 remained insensitive to FSK/IBMX treatment (n = 2 experiments; 10 mito-GO-ATeam3 cells). (C) Mito-GO-ATeam2 responded to cytosolic cAMP increases induced by FSK/IBMX; however, no additional increase in ATP production was observed when we added high concentrations of the cell-permeant cAMP analogue 8CPT-cAMP, which was expected to activate matrix-located cAMP-sensitive pathways. Data are shown from a single representative experiment out of six repeats (28 mito-GO-ATeam2 cells). (D) Bar graph summarizing the effects on mitochondrial ATP content in HeLa cells transfected for 24 h with mito-GO-ATeam2 alone (control) or together with mito-PKI mCherry ("mito-PKI"), mito-PKACat(a)mCherry ("mito-PKA"), cyto-PKI-mCherry ("cyto-PKI"), or cyto-PKACat(a)mCherry ("cyto-PKA"). ATP content was assessed by measuring the change in the FRET ratio after acute treatment with the mitochondrial uncoupler FCCP. Data are from at least four independent experiments for each condition. Error bars indicate mean ± SD.